PHYSICS

Optimal repetitive readout of single solid-state spins determined by Fisher information

Zhiyuan Zhao[1,2,3]†, Shaoyi Xu[1,2,3]†, Qian Shi[1,2,3], Yu Chen[1,2,3], Xi Kong[4], Zhiping Yang[1,2,5], Mengqi Wang[1,2,3], Xiangyu Ye[1,2,3], Pei Yu[1,2,3], Ya Wang[1,2,3,6], Tianyu Xie[1,2,3]*, Fazhan Shi[1,2,3,5,6]*, Jiangfeng Du[1,2,3,6,7]*

Quantum systems, including superconducting circuits, trapped ions, quantum dots, solid-state defects, etc., have achieved considerable advancements in readout fidelity. However, the widely used threshold method disregards the importance of temporal characteristics of the signal during continuous measurements, leading to information loss. Here, we applied Fisher information to quantify the potential enhancement by using the temporal information. We proposed an optimal data processing method and derived the condition for equality to the error constrained by Fisher information. Applying this method to the single-shot readout of a ^{13}C nuclear spin of nitrogen-vacancy center marks a 33.8 ± 1.2% error reduction compared to the threshold method, improving the fidelity to 99.649(5)%. The versatility of our method is further demonstrated through the single-shot readout of charge states. This work illustrates the advantage of using photon arrival time for improving readout fidelity without upgrading experimental hardware. The method of using Fisher information to analyze readout fidelity also holds promise for broad applicability to other systems.

INTRODUCTION

Single-shot readout of qubits is a cornerstone technology in quantum information processing, especially fault-tolerant quantum computation (*1*–*3*). It has been successfully realized across various physical systems, such as trapped ions (*4*, *5*), neutral atoms (*6*, *7*), superconducting circuits (*8*, *9*), quantum dots (*10*, *11*), and solid-state defects (*10*, *12*). Typical methods for processing single-shot measurements adopt a threshold strategy in which two states are distinguished by a preset threshold (*12*–*14*). However, such threshold methods fail to incorporate the temporal information.

Several studies have endeavored to improve readout fidelity (*4*, *15*–*18*) and readout speed (*19*, *20*) by considering this unrecognized aspect. Most of the existing studies to improve the fidelity concentrate primarily on model-based derivations and numerical simulations (*15*–*18*), with experimental verifications being relatively sparse. Machine learning is also applied to mine the hidden information in photon arrival time (*21*), but it does not gain substantial improvements in fidelity and lacks a rigorous explanation in theory.

To fully address the issues above, we analyzed the theoretical upper bound of readout fidelity by harnessing the framework of Fisher information (*22*), which avoids pursuing different methods without a solid theoretical foundation. Subsequently, we proposed the optimal data processing method and derived the condition for equality to the error constrained by Fisher information. The method was validated experimentally by two kinds of single-shot readouts in a nitrogen-vacancy (NV) center, specifically, spin states of a nuclear spin and NV charge states. The theoretical framework established in this work for using photon arrival time to enhance readout fidelity is broadly applicable to a wide variety of quantum systems.

SYSTEM AND THEORETICAL MODEL

As shown in Fig. 1A, the NV center is a point defect in diamond where a substitutional nitrogen atom is adjacent to a vacancy. It is characteristic of optical accessibility (*23*), long-lived quantum coherence (*24*, *25*), high-fidelity manipulation (*26*, *27*), and susceptibility to various physical quantities (*28*, *29*). These excellent properties make it an ideal candidate for a variety of quantum applications ranging from quantum network (*30*, *31*) to quantum sensing (*32*–*35*).

The optical readout of the NV electron spin is performed by detecting the spin-dependent fluorescence arising from excited-state intersystem crossing. Nevertheless, the NV electron spin becomes repolarized within several hundred nanoseconds under laser illumination, so that the number of the collected photons in a single readout is typically less than one for room temperature measurements (*36*), even with high-efficiency collection structures (*37*, *38*). To collect more photons, the nuclear-assisted repetitive readout was proposed by using the fact that the nuclear spin lifetime under laser illumination largely exceeds that of the electron spin (*39*). Under a high magnetic field for further extending the lifetime, the method of repetitive readout eventually enables single-shot readout of nuclear spins (*12*), which is indispensable in the realization of quantum error-correction codes (*40*). In this context, single-shot readout refers to the ability to read out the nuclear spin state after a single initialization, without the need to reinitialize the nuclear spin.

The implementation sequence of repetitive readout is presented in the inset of Fig. 1B. The nuclear spin state is read out repetitively by correlating the nuclear spin with the NV electron spin using a

[1]CAS Key Laboratory of Microscale Magnetic Resonance and School of Physical Sciences, University of Science and Technology of China, Hefei 230026, China. [2]Anhui Province Key Laboratory of Scientific Instrument Development and Application, University of Science and Technology of China, Hefei 230026, China. [3]CAS Center for Excellence in Quantum Information and Quantum Physics, University of Science and Technology of China, Hefei 230026, China. [4]National Laboratory of Solid State Microstructures and Department of Physics, Nanjing University, Nanjing 210093, China. [5]School of Biomedical Engineering and Suzhou Institute for Advanced Research, University of Science and Technology of China, Suzhou 215123, China. [6]Hefei National Laboratory, University of Science and Technology of China, Hefei 230088, China. [7]School of Physics, Zhejiang University, Hangzhou 310027, China.
*Corresponding author. Email: xie1021@ustc.edu.cn (T.X.); fzshi@ustc.edu.cn (F.S.); djf@ustc.edu.cn (J.D.)
†These authors contributed equally to this work.

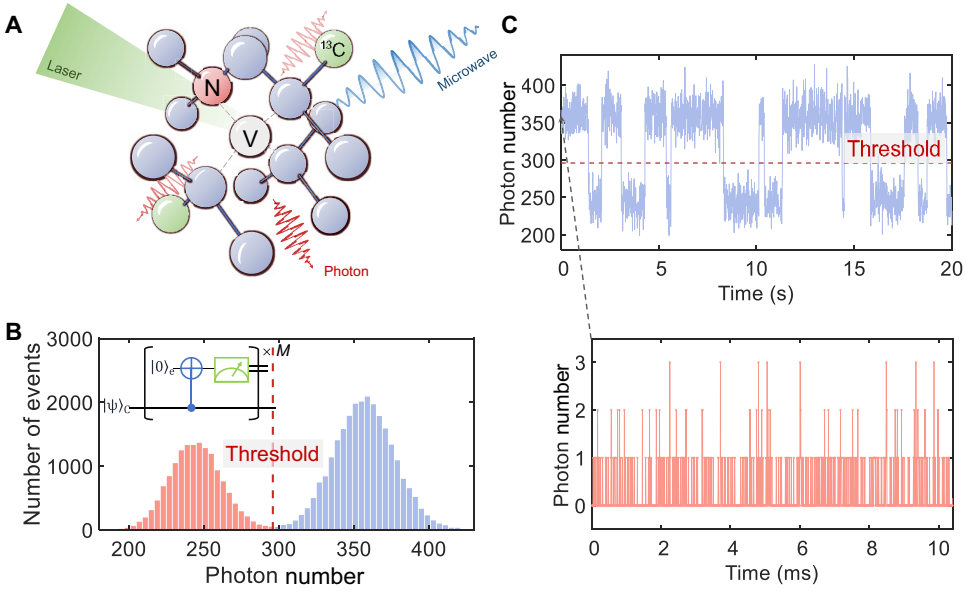

Fig. 1. Single-shot readout based on repetitive readout. (**A**) Diagram of the NV center and its proximal nuclear spins. Please see Materials and Methods for detailed information about the sample and platform. (**B**) Typical single-shot readout sequence and results of a ^{13}C nuclear spin. Each event here is the result of the summation of $M = 1300$ cycles, from which the nuclear spin state is determined based on a threshold. (**C**) Readout trajectory of a ^{13}C spin near the NV center. The lower subplot displays the original data of the first point in the upper one.

controlled-NOT (C_nNOT_e) gate. With the threshold method adopted, every $M = 1300$ readout results are directly combined cumulatively to produce a two-peak histogram in Fig. 1B for mapping the photon number into the corresponding state by comparing with a threshold. Here, M is the number of readouts in a single-shot measurement. However, the threshold method with a simple summation discards a large amount of temporal information of photon arrival, as clearly shown in Fig. 1C.

The error bound determined by Fisher information

Instead of proposing an alternative method, we first introduce Fisher information to quantify the space for improving the readout fidelity. Considering a random variable that follows a probability distribution incorporating a parameter s, $P(x\,|\,s)$. The variance of an unbiased estimator $\hat{S}$ of the parameter s is then bounded by

$$(\Delta s)^2 = \mathrm{Var}\left(\hat{S}\right) \geq \frac{1}{F(s)} \tag{1}$$

where the Fisher information $F(s)$ is given by $F(s) = \sum_x P(x\,|\,s)\left(\frac{\partial \ln P(x|s)}{\partial s}\right)^2$. The lower bound provided by Eq. 1 is known as the Cramér-Rao bound, and the amount of Fisher information determines the optimal measurement precision. The initial state before readout follows the distribution $P_s(n_1, n_2, \ldots, n_N) = \frac{1+s}{2}P_+(n_1, n_2, \ldots, n_N) + \frac{1-s}{2}P_-(n_1, n_2, \ldots, n_N)$, where $P_+(n_1, n_2, \ldots, n_N)$ and $P_-(n_1, n_2, \ldots, n_N)$ are the distributions of bright state $|+\rangle$ and dark state $|-\rangle$ respectively. Here, n_i denotes the photon counts of the ith segment, and s ranges from -1 to $+1$. For brevity, we denote these symbols as $P_{s/+/-}(\boldsymbol{n})$ with $\boldsymbol{n} = (n_1, n_2, \ldots, n_N)$. In a single-shot readout, N represents the number of segments, with each segment containing M/N readout cycles. Given that most cycles yield no photons, processing each cycle's data individually is not necessary. We thus group the total readout cycles into several cumulative time-domain segments (see Fig. 2A). Notably, with the data divided into about 10 segments, performance effectively approaches saturation (see the Supplementary Materials for details).

Considering the variance of the estimator after state mapping (see Materials and Methods), a constraint to the readout error ε_r at $s = 0$ is given by

$$\left(1 - 2\varepsilon_r\right)^2 \leq F = 1 - I \tag{2}$$

where I is the overlap integral of the bright state and the dark state distribution (*22*), and reads

$$I = \sum_{\boldsymbol{n}} \frac{2P_+(\boldsymbol{n})P_-(\boldsymbol{n})}{P_+(\boldsymbol{n}) + P_-(\boldsymbol{n})} \tag{3}$$

Therefore, computing the lower bound of ε_r is converted into the calculation of the overlap integral

$$\varepsilon_r \geq \frac{1 - \sqrt{1 - I}}{2} = \varepsilon_0 \tag{4}$$

where ε_0 is the error constrained by Fisher information. However, calculating the overlap integral is not a trivial task as its computational complexity grows exponentially with N. To solve this issue, the method of random sampling is adopted here (see Materials and Methods).

Attainability of the Fisher information bound

In this subsection, we discuss the maximum likelihood method and the attainability of the Fisher information bound. In the readout process, if the initial state is the bright state $|+\rangle$, after N readout segments, the probability of flipping from $|+\rangle$ to $|-\rangle$ is denoted as ϵ_{+-}. This makes nonflipping probability $1 - \epsilon_{+-}$, and the flipping probability per readout segment ϵ_{+-}/N, assuming that the probability of flipping is small. In a

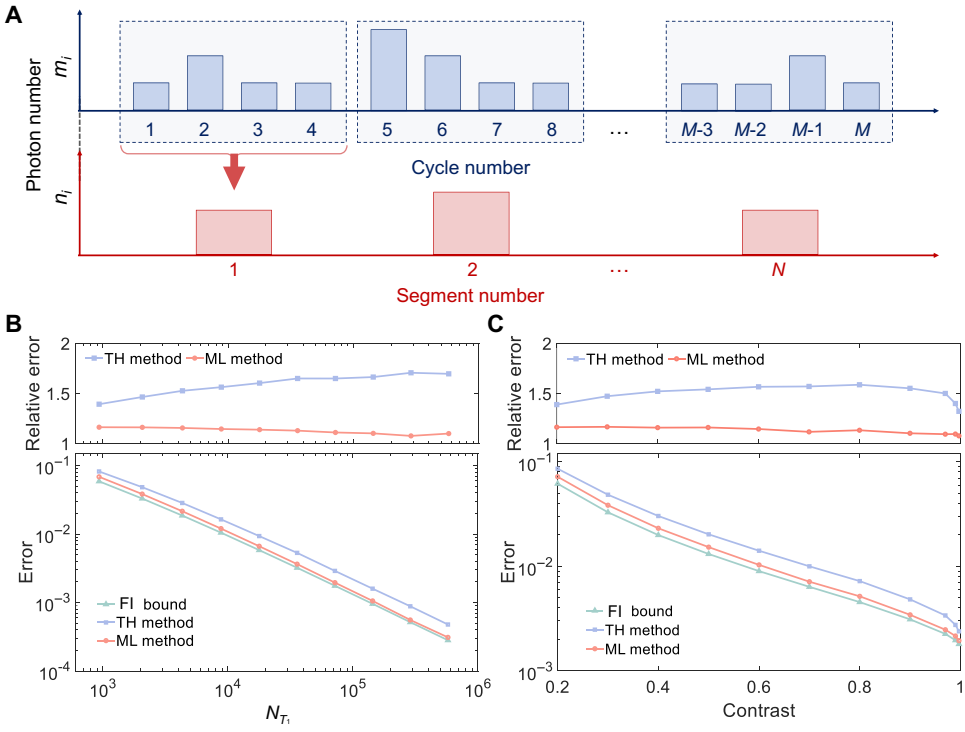

Fig. 2. Simulation of single-shot readout error. (**A**) Segmentation of data in our method. In this diagram, a single-shot readout with M cycles is divided into N segments, each with M/N cycles. The figure takes $M/N = 4$ as an example. m_i represents the number of photons in the ith readout cycle, while n_i denotes the sum of photons for the ith segment. (**B**) Single-shot readout error versus the number of fluorescence photons collected within the lifetime of states N_{T_1}. T_1 is the lifetime of states (the mean number of readouts without state flipping). The green line corresponds to the lower bound ε_0 determined by Fisher information (FI bound), the blue line is the readout error using the threshold method (TH method), and the red line is the readout error based on the maximum likelihood estimation (ML method). The upper figure depicts the errors relative to the FI bound. The contrast here is fixed to 0.32. (**C**) Single-shot readout error under different readout contrasts. The readout contrast is defined as one minus the average count of the dark state over that of the bright one. Here, N_{T_1} is set to 2.42×10^3.

similar manner, if the initial state is the dark state $|-\rangle$, the same logic can be used by simply swapping + and – in the above description. For the ith readout, the collected photon count n_i follows a Poisson distribution

$$p_{+/-}(n_i) = \frac{\lambda_{+/-}^{n_i}}{n_i!} e^{-\lambda_{+/-}}, n_i = 0, 1, \ldots \tag{5}$$

where $\lambda_{+/-}$ is the average count of the bright/dark state. However, if state flipping takes place in a certain segment, it is inaccurate to approximate the distribution of this group with Eq. 5. The photon count then follows the mixed Poisson distribution

$$p(n_i) = \frac{\gamma(n_i+1, \lambda_+) - \gamma(n_i+1, \lambda_-)}{n_i!(\lambda_+ - \lambda_-)}, n_i = 0, 1, \ldots \tag{6}$$

where γ refers to the lower incomplete gamma function: $\gamma(n, \lambda) = \int_0^\lambda t^{n-1} e^{-t} dt$.

On the basis of the aforementioned model, we can write the likelihood function for N successive readouts as

$$P_+(\boldsymbol{n}) = \frac{\epsilon_{+-}}{N} \sum_{i=1}^{N} p(n_i) \prod_{j=1}^{i-1} p_+(n_j) \prod_{j=i+1}^{N} p_-(n_j) + (1-\epsilon_{+-}) \prod_{j=1}^{N} p_+(n_j) \tag{7}$$

$$P_-(\boldsymbol{n}) = \frac{\epsilon_{-+}}{N} \sum_{i=1}^{N} p(n_i) \prod_{j=1}^{i-1} p_-(n_j) \prod_{j=i+1}^{N} p_+(n_j) + (1-\epsilon_{-+}) \prod_{j=1}^{N} p_-(n_j) \tag{8}$$

This model provides a precise representation of the single-shot readout process. On the basis of this, we can formulate a criterion by using maximum likelihood estimation

$$\Lambda = \frac{P_+}{P_-} \tag{9}$$

When $\Lambda \geq 1$, the state is classified as the bright state; otherwise, it is classified as the dark one. The error of maximum likelihood criterion is

$$\varepsilon_m = \frac{1}{2} \sum_{\boldsymbol{n}} \min\{P_+(\boldsymbol{n}), P_-(\boldsymbol{n})\} \tag{10}$$

As proved in the Supplementary Materials, the method of maximum likelihood estimation is the optimal for state mapping, with the error ε_m bounded by Eq. 4

$$\varepsilon_m \geq \varepsilon_0 \tag{11}$$

The equality can be reached under the condition

$$\max\left\{\frac{P_+}{P_-},\frac{P_-}{P_+}\right\}\Big|_{\boldsymbol{n}} = C \tag{12}$$

where C is a constant for all $\boldsymbol{n}$ (see a detailed derivation in Materials and Methods). The fact that the equality in Eq. 11 can be achieved suggests that under some specific cases, the process of state mapping can be conducted without Fisher information loss, which differs from the conclusion of the previous work (*22*). However, it is challenging to meet the equality condition in Eq. 12, and hence a realistic single-shot readout fails to exactly reach the error ε_0 given by Fisher information.

For realistic systems, the readout error mainly depends on three factors, the contrast between bright and dark states, the count per readout, and the lifetime of states T_1 (chosen to be equal for two states in the simulation). The latter two factors can be combined into a single parameter: the number of fluorescence photons collected within the lifetime of states N_{T_1}. For single NV centers, the contrast between bright and dark states is approximately 0.3. The readout error ε_0 determined by Fisher information is numerically calculated as well as those from the threshold method and the maximum likelihood estimation, with results shown in Fig. 2B. The maximum likelihood estimation can approach ε_0, while the threshold method deviates at a distance. The readout errors under different contrasts are also calculated in Fig. 2C, with the contrast greater than 0.9 corresponding to the scenarios for reading out NV charge states (*41*, *42*) and internal states of atoms (*4*–*7*). Likewise, the method of maximum likelihood estimation draws near ε_0 and exhibits an observable improvement over the threshold method.

RESULTS

We conducted experiments on the NV center to verify the effectiveness of the theoretical analysis above. On the basis of a home-built platform of optically detected magnetic resonance, we collected data of the single-shot readout of a ^{13}C nuclear spin under a high magnetic field (~9199 G). The state initialization is implemented through the postselection of single-shot readout results (see details in Materials and Methods and fig. S4). The process of state mapping is executed in accordance with the schematic procedures in Fig. 3A. For the threshold method, fidelity initially increases but then slightly decreases as the number of readouts grows. This reduction in fidelity is attributed to state flips induced by the readout process, thereby increasing the readout error (which still remains small; otherwise, single-shot readout would be unattainable). In contrast, the method of maximum likelihood estimation is capable of maintaining the highest readout fidelity over a broader range. The proposed method enhances fidelities by extending data acquisition times through accounting for potential spin flips. Eventually in our experiments, we achieved a 99.649(5)% readout fidelity for the nuclear spin, marking a 33.8 ± 1.2% error reduction compared to the threshold method at the optimal number of readouts. Our single-shot readout fidelity exceeds 99.5%, reliably surpassing the threshold required for efficient error correction, estimated to be approximately 0.5% for achieving the break-even point (*43*). The analysis and correction of systematic deviations are included in Materials and Methods.

Our method can be universally applied to more single-shot readout cases. We use the single-shot readout of NV charge states as another example (*41*, *42*). It has been achieved by using the mechanism that the

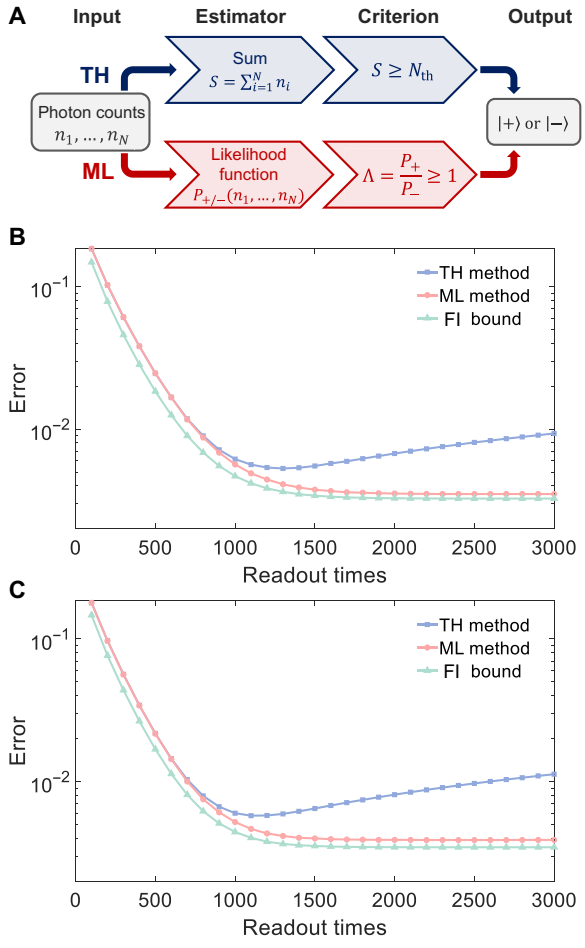

Fig. 3. Single-shot readout error of a ^{13}C nuclear spin adjacent to the NV center. (**A**) The procedure of data processing using the TH method and the ML method. N_{th} is the threshold in Fig. 1B. Both the readout times and the threshold have been optimized. $P_{+/-}$ is the likelihood function of bright/dark state, and see Eqs. 7 and 8 for details. (**B**) Experimental results of single-shot readout errors for different methods. The horizontal axis represents the number of readout cycles. Details of the initialization and experimental parameters can be found in Materials and Methods. For the TH method, the error increases for too many readout times due to state flipping. (**C**) Simulation results for different methods.

594-nm laser only excites NV^-, but not NV^0 (*44*). The sequence is shown in Fig. 4A with a 50-μs duration as a readout cycle. Because the single-shot readout of NV charge states rather resembles the cases of reading out internal states of atoms (*4*–*7*), the universality of this method applied to other physical systems is further validated through the experiment. A readout fidelity of 99.741(4)% is lastly achieved for the single-shot readout of NV charge states, corresponding to a 22.4 ± 1.6% decrease in error compared to the threshold method. The experimental results and the simulations are consistent on the whole, as shown in Fig. 4 (B and C). The main difference stems from the fact that the actual distribution of photon number fluctuates slightly larger than the corresponding Poisson distribution for the dark state.

DISCUSSION

In conclusion, we conducted a quantitative analysis of the potential fidelity enhancement based on Fisher information theory. The

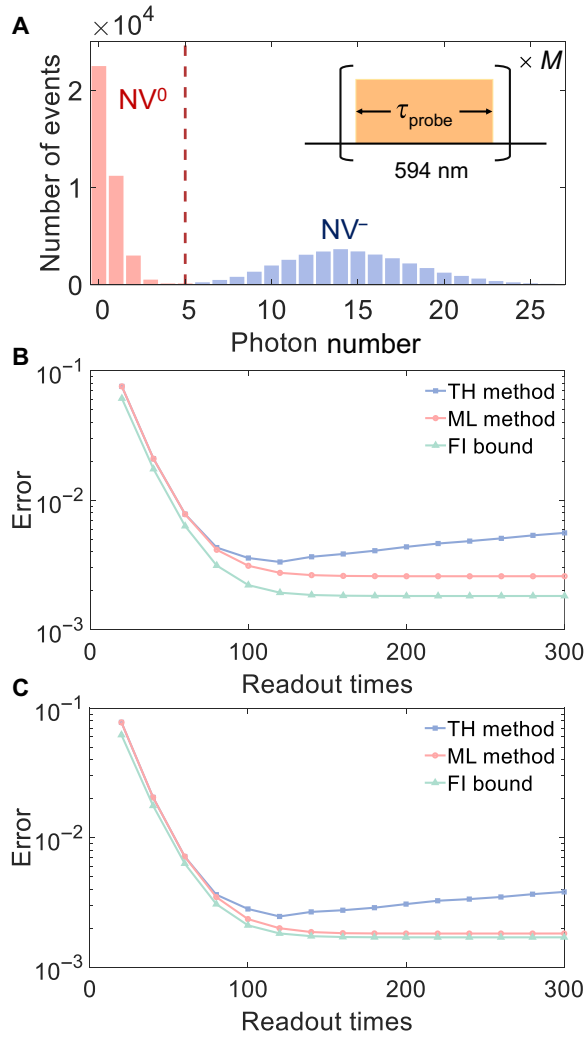

Fig. 4. Single-shot readout of NV charge state. (**A**) Statistical histogram of charge state readout based on the threshold method. The subplot shows the sequence of charge state single-shot readout. Each event here is the result of the summation of 100 readout cycles. Each cycle is a 50-μs 594-nm laser illumination. (**B**) Experimental results of single-shot readout of charge state. Details of the experimental sequences and parameters can be found in fig. S2 and the Supplementary Materials. (**C**) Simulation results of charge state readout.

method based on maximum likelihood estimation was used here with its optimality proved rigorously, and most importantly, the condition for equality to the error constrained by Fisher information was derived. Furthermore, the above findings in theory were verified experimentally with single-shot readouts of a ^{13}C nuclear spin and charge states of the NV center. The method of maximum likelihood estimation can approach the error constrained by Fisher information and exhibits higher fidelities compared to the threshold method. While the observed improvements may be moderate, the primary advantage of our proposed optimal readout scheme is its ability to enhance readout fidelity within existing experimental setups without the need for additional experimental equipment or complex hardware upgrades, as it leverages the temporal information of photon arrival. Besides, our method can address not only spin flips but also the error associated with the $C_n NOT_e$ gate. The impacts of these errors have been integrated into the parameters, i.e., fluorescence counts, the lifetime of states, and the contrast within the existing model.

Our method provides a general theoretical framework for analyzing potential improvements of readout fidelity using Fisher information and avoids the indiscriminate trial of various methods without a solid foundation. Although demonstrated in a solid-state spin system, the versatility of our method and theoretical framework allows them to be extended to enhance the readout fidelity in other quantum systems, such as trapped ions (*4*, *5*), neutral atoms (*6*, *7*), and quantum dots (*10*, *11*). For instance, in the case of quantum dot readout, the photon number distribution in our model can be replaced with the corresponding one in the literature (*10*, *11*). Especially considering the widespread use of the threshold method in systems that have already achieved substantial advancements in readout fidelity and efficiency (*45*, *46*), it is more worthwhile to adopt our strategies to further improve readout performance.

MATERIALS AND METHODS

Diamond sample and experimental setup

The diamond used in the experiment is synthesized through chemical vapor deposition, with a nitrogen concentration less than 5 parts per billion and natural abundance (1.1%) ^{13}C. The top face of the diamond is perpendicular to the [100] crystal axis, while the lateral faces are perpendicular to the [110] axis. The diamond is irradiated by 1.0 kGy (kilogray) 10-MeV electrons. Solid immersion lenses are etched on the top face to increase the photon collection efficiency, and the count rates of NV centers used in the experiments are 650 to 850 kcounts/s. The simplified experimental setup is illustrated in fig. S1. Details of experimental setup can be seen in the Supplementary Materials.

The error constrained by fisher information

Let $P(x\,|\,s)$ be the probability distribution function with a parameter s, and then the Fisher information $F(s)$ is given by

$$F(s) = \sum_x P(x\,|\,s)\left(\frac{\partial \ln P(x\,|\,s)}{\partial s}\right)^2 \tag{13}$$

By substituting $P_s(\boldsymbol{n}) = \frac{1+s}{2}P_+(\boldsymbol{n}) + \frac{1-s}{2}P_-(\boldsymbol{n})$, it can be obtained that (*22*)

$$F(s) = \frac{1}{1-s^2} - \frac{1}{1-s^2}I(s), \quad I(s) = \sum_{\boldsymbol{n}} \frac{P_+(\boldsymbol{n})P_-(\boldsymbol{n})}{P_s(\boldsymbol{n})} \tag{14}$$

Because the probability of the bright state after state mapping is $\hat{p}_+(s) = \frac{1+s}{2}\cdot(1-\varepsilon_+) + \frac{1-s}{2}\cdot\varepsilon_-$, the unbiased estimator for s can be given in the following form

$$\hat{S} = 2\cdot\frac{\hat{p}_+ - \varepsilon_-}{1-2\varepsilon_r} - 1 \tag{15}$$

where $\hat{p}_+ = \frac{\hat{N}_+}{N}$ is the estimator for the ratio of the bright state after state mapping. ε_+ and ε_- are the readout errors for the bright state and the dark state, respectively. Considering the variance after state mapping, a constraint to the readout error ε_r at $s = 0$ is given by

$$(\Delta s)^2 = \mathrm{Var}\left(\hat{S}\right) = \frac{4}{\left(1-2\varepsilon_r\right)^2}\mathrm{Var}\left(\hat{p}_+\right) = \frac{1-\left(\varepsilon_+-\varepsilon_-\right)^2}{\left(1-2\varepsilon_r\right)^2} \geq \frac{1}{F} \tag{16}$$

Consequently

$$\frac{1}{\left(1-2\varepsilon_r\right)^2} \geq \frac{1-\left(\varepsilon_+-\varepsilon_-\right)^2}{\left(1-2\varepsilon_r\right)^2} \geq \frac{1}{F} \tag{17}$$

Therefore, computing the lower bound of readout error ε_r is converted into the calculation of the overlap integral I

$$\varepsilon_r \geq \frac{1-\sqrt{1-I}}{2} = \varepsilon_0 \tag{18}$$

where ε_0 is the error constrained by Fisher information.

Attainability of the Fisher information bound

The lower bound of the readout error determined by the Fisher information is

$$\varepsilon_0 = \frac{1-\sqrt{1-I}}{2}, \quad I = \sum_{\boldsymbol{n}} \frac{2P_+P_-}{P_++P_-} \tag{19}$$

It can be proven that

$$\varepsilon_0 \leq \varepsilon_m \tag{20}$$

Proof

$$\begin{aligned}
&\varepsilon_0 \leq \varepsilon_m \\
\Leftrightarrow &1-\sum_{\boldsymbol{n}} \min\{P_+,P_-\} \leq \sqrt{1-I} \\
\Leftrightarrow &\left(1-\sum_{\boldsymbol{n}} \min\{P_+,P_-\}\right)^2 \leq 1-\sum_{\boldsymbol{n}} \frac{2P_+P_-}{P_++P_-} \\
\Leftrightarrow &\left(\sum_{\boldsymbol{n}} \frac{P_++P_-}{2}-\min\{P_+,P_-\}\right)^2 \leq \sum_{\boldsymbol{n}} \frac{P_++P_-}{2}-\frac{2P_+P_-}{P_++P_-} \\
\Leftrightarrow &\left(\sum_{\boldsymbol{n}} \frac{P_++P_-}{2}-\min\{P_+,P_-\}\right)^2 \leq \left(\sum_{\boldsymbol{n}} \frac{P_++P_-}{2}-\frac{2P_+P_-}{P_++P_-}\right)\cdot 1 \\
\Leftrightarrow &\left(\sum_{\boldsymbol{n}} \frac{|P_+-P_-|}{2}\right)^2 \leq \left(\sum_{\boldsymbol{n}} \frac{\left(P_+-P_-\right)^2}{2\left(P_++P_-\right)}\right)\cdot\left(\sum_{\boldsymbol{n}} \frac{P_++P_-}{2}\right)
\end{aligned} \tag{21}$$

In the proof, the trick of substituting $\sum_{\boldsymbol{n}} \frac{P_++P_-}{2}$ for the number "1" is used three times. According to the Cauchy-Schwarz inequality, the aforementioned inequality holds, and the equality can be reached under the condition

$$\max\left\{\frac{P_+}{P_-},\frac{P_-}{P_+}\right\}\Big|_{\boldsymbol{n}} = C \tag{22}$$

for all $\boldsymbol{n}$, where C is a constant and $\varepsilon_0 = \varepsilon_m = 1/(1+C)$. That is to say, under special conditions, the Fisher information does not diminish after state mapping. Herein, we present a special case that fulfills Eq. 22 in Table 1, where for all $\boldsymbol{n}$, the condition $\max\left\{\frac{P_+}{P_-},\frac{P_-}{P_+}\right\}\Big|_{\boldsymbol{n}} = 3$ holds, $\varepsilon_0 = \varepsilon_m = 1/4$. However, the condition is nearly impossible to be attained in a practical experiment. Thus, while the maximum likelihood estimation is the optimal method that can attain the error ε_0 given by Fisher information theoretically, the method fails to reach it exactly in a realistic experiment.

Calculation of the overlap integral

The upper bound of readout fidelity can be obtained from the overlap integral. However, calculating the overlap integral is not trivial as its computational complexity grows exponentially with N. Numerical computations become particularly challenging for standard computers when $N > 4$.

To mitigate this computational difficulty, we adopt a method of random sampling. From another perspective, I essentially represents the weighted average of $\frac{2P_-}{P_++P_-}$ with respect to P_+. It is more intuitive to express the overlapping integral I as

$$I = \sum_{\boldsymbol{n}} P_+ \cdot \frac{2P_-}{P_++P_-} \tag{23}$$

For the readout data whose initial state is $|+\rangle$ ($|-\rangle$), computing the average value of $\frac{2P_-}{P_++P_-}\left(\frac{2P_+}{P_++P_-}\right)$ will yield the overlapping integral I. The convergence of this random sampling method is good, greatly reducing the computational complexity and enabling numerical calculation of the overlapping integrals.

State initialization

The initialization of the state is implemented through the postselection of single-shot readout results. As depicted in fig. S4, the initialization of bright/dark states can be achieved by adjusting the threshold to a higher/lower setting. If a readout result meets the threshold condition, the initial state can be determined. The selected data are segments of photon data after this readout. Despite this process involving the discarding of a great quantity of data, the state can nevertheless be initialized with high fidelity if an appropriate threshold is set. For the bright and dark states of the nuclear spin, we respectively obtained 1,796,698 and 846,621 groups of valid data after initialization. For the charge state, we obtained 55,604,864 and 807,683 groups of valid data after initialization.

Systematic deviation induced by imperfect initialization

In the data processing process, we have assumed that the initialization is perfect. Here, we estimate the system bias brought by this assumption. The initialization error can be quantified by analyzing the overlap of the photon distributions. For the initialization of the dark state, the imperfection of the initialization process is

Table 1. A case for attaining the Fisher information bound.

№	n_1	n_2	n_3	n_4	n_5
P_+	135/484	23/242	24/121	75/484	3/11
P_-	45/484	69/242	8/121	225/484	1/11

$$\epsilon_-^{\mathrm{ini}} = \frac{R_-\epsilon_{-+}S_f + R_+\left(1-\epsilon_{+-}\right)S_+}{R_-\epsilon_{-+}S_f + R_+\left(1-\epsilon_{+-}\right)S_+ + R_+\epsilon_{+-}S_f + R_-\left(1-\epsilon_{-+}\right)S_-}$$
$$\approx \frac{\epsilon_{-+}S_f}{\epsilon_{-+}S_f + \left(1-\epsilon_{-+}\right)S_- + \frac{R_+}{R_-}\epsilon_{+-}S_f} \quad (24)$$
$$\approx \frac{\epsilon_{-+}S_f}{\epsilon_{-+}S_f + \left(1-\epsilon_{-+}\right)S_-}$$

where $S_f = \sum_{n=0}^{k} p(n)$, $S_+ = \sum_{n=0}^{k} p_+(n)$, and $S_- = \sum_{n=0}^{k} p_-(n)$. R_+/R_- is the population of the bright/dark state before initialization, n is the summed count over the duration of readout, and k is the initialization threshold. The first approximation holds because the overlap of photon distribution between the dark state and the bright state can be ignored ($S_+ < 10^{-14}$ for nuclear spin readout). The second approximation comes from the fact that $S_- \gg S_f$, $R_+/R_- \approx 1$, and $\epsilon_{+-} \ll 1$. When the initialization threshold for the dark state is selected as 220, $\epsilon_-^{\mathrm{ini}}$ is $9.0(3) \times 10^{-4}$; similarly, for the bright state, the threshold is selected as 390, and $\epsilon_+^{\mathrm{ini}}$ is $4.7(2) \times 10^{-4}$. The charge state initialization is similar (as shown in fig. S4). When the initialization thresholds for the bright and dark states are set to 24 and 1, the initialization errors are $1.01(5) \times 10^{-3}$ and $5.5(4) \times 10^{-5}$, respectively. The correction of systematic deviation can be seen in the Supplementary Materials.

Supplementary Materials

This PDF file includes:

Supplementary Text
Figs. S1 to S5
Table S1

REFERENCES AND NOTES

1. E. T. Campbell, B. M. Terhal, C. Vuillot, Roads towards fault-tolerant universal quantum computation. *Nature* **549**, 172–179 (2017).
2. J. M. Chow, J. M. Gambetta, E. Magesan, D. W. Abraham, A. W. Cross, B. R. Johnson, N. A. Masluk, C. A. Ryan, J. A. Smolin, S. J. Srinivasan, M. Steffen, Implementing a strand of a scalable fault-tolerant quantum computing fabric. *Nat. Commun.* **5**, 4015 (2014).
3. B. J. Brown, S. Roberts, Universal fault-tolerant measurement-based quantum computation. *Phys. Rev. Res.* **2**, 033305 (2020).
4. A. H. Myerson, D. J. Szwer, S. C. Webster, D. T. C. Allcock, M. J. Curtis, G. Imreh, J. A. Sherman, D. N. Stacey, A. M. Steane, D. M. Lucas, High-fidelity readout of trapped-ion qubits. *Phys. Rev. Lett.* **100**, 200502 (2008).
5. T. Harty, D. Allcock, C. J. Ballance, L. Guidoni, H. Janacek, N. Linke, D. Stacey, D. Lucas, High-fidelity preparation, gates, memory, and readout of a trapped-ion quantum bit. *Phys. Rev. Lett.* **113**, 220501 (2014).
6. I. S. Madjarov, A. Cooper, A. L. Shaw, J. P. Covey, V. Schkolnik, T. H. Yoon, J. R. Williams, M. Endres, An atomic-array optical clock with single-atom readout. *Phys. Rev. X* **9**, 041052 (2019).
7. R. Gehr, J. Volz, G. Dubois, T. Steinmetz, Y. Colombe, B. L. Lev, R. Long, J. Esteve, J. Reichel, Cavity-based single atom preparation and high-fidelity hyperfine state readout. *Phys. Rev. Lett.* **104**, 203602 (2010).
8. P. Krantz, A. Bengtsson, M. Simoen, S. Gustavsson, V. Shumeiko, W. Oliver, C. Wilson, P. Delsing, J. Bylander, Single-shot read-out of a superconducting qubit using a josephson parametric oscillator. *Nat. Commun.* **7**, 11417 (2016).
9. T. Walter, P. Kurpiers, S. Gasparinetti, P. Magnard, A. Potočnik, Y. Salathé, M. Pechal, M. Mondal, M. Oppliger, C. Eichler, A. Wallraff, Rapid high-fidelity single-shot dispersive readout of superconducting qubits. *Phys. Rev. Appl.* **7**, 054020 (2017).
10. A. Morello, J. J. Pla, F. A. Zwanenburg, K. W. Chan, K. Y. Tan, H. Huebl, M. Möttönen, C. D. Nugroho, C. Yang, J. A. Van Donkelaar, A. D. C. Alves, D. N. Jamieson, C. C. Escott, L. C. L. Hollenberg, R. G. Clark, A. S. Dzurak, Single-shot readout of an electron spin in silicon. *Nature* **467**, 687–691 (2010).
11. A. West, B. Hensen, A. Jouan, T. Tanttu, C.-H. Yang, A. Rossi, M. F. Gonzalez-Zalba, F. Hudson, A. Morello, D. J. Reilly, A. S. Dzurak, Gate-based single-shot readout of spins in silicon. *Nat. Nanotechnol.* **14**, 437–441 (2019).
12. P. Neumann, J. Beck, M. Steiner, F. Rempp, H. Fedder, P. R. Hemmer, J. Wrachtrup, F. Jelezko, Single-shot readout of a single nuclear spin. *Science* **329**, 542–544 (2010).
13. A. Dréau, P. Spinicelli, J. Maze, J.-F. Roch, V. Jacques, Single-shot readout of multiple nuclear spin qubits in diamond under ambient conditions. *Phys. Rev. Lett.* **110**, 060502 (2013).
14. G.-Q. Liu, J. Xing, W.-L. Ma, P. Wang, C.-H. Li, H. C. Po, Y.-R. Zhang, H. Fan, R.-B. Liu, X.-Y. Pan, Single-shot readout of a nuclear spin weakly coupled to a nitrogen-vacancy center at room temperature. *Phys. Rev. Lett.* **118**, 150504 (2017).
15. J. Gambetta, W. Braff, A. Wallraff, S. Girvin, R. Schoelkopf, Protocols for optimal readout of qubits using a continuous quantum nondemolition measurement. *Phys. Rev. A* **76**, 012325 (2007).
16. S. Ng, M. Tsang, Optimal signal processing for continuous qubit readout. *Phys. Rev. A* **90**, 022325 (2014).
17. B. D'Anjou, W. A. Coish, Optimal post-processing for a generic single-shot qubit readout. *Phys. Rev. A* **89**, 012313 (2014).
18. B. D'Anjou, W. A. Coish, Enhancing qubit readout through dissipative sub-Poissonian dynamics. *Phys. Rev. A* **96**, 052321 (2017).
19. B. D'Anjou, L. Kuret, L. Childress, W. A. Coish, Maximal adaptive-decision speedups in quantum-state readout. *Phys. Rev. X* **6**, 011017 (2016).
20. X. Xue, B. D'Anjou, T. F. Watson, D. R. Ward, D. E. Savage, M. G. Lagally, M. Friesen, S. N. Coppersmith, M. A. Eriksson, W. A. Coish, L. M. K. Vandersypen, Repetitive quantum nondemolition measurement and soft decoding of a silicon spin qubit. *Phys. Rev. X* **10**, 021006 (2020).
21. G. Liu, M. Chen, Y.-X. Liu, D. Layden, P. Cappellaro, Repetitive readout enhanced by machine learning. *Mach. Learn. Sci. Technol.* **1**, 015003 (2020).
22. B. D'Anjou, W. A. Coish, Soft decoding of a qubit readout apparatus. *Phys. Rev. Lett.* **113**, 230402 (2014).
23. A. Gruber, A. Drabenstedt, C. Tietz, L. Fleury, J. Wrachtrup, C. von Borczyskowski, Scanning confocal optical microscopy and magnetic resonance on single defect centers. *Science* **276**, 2012–2014 (1997).
24. T. Yamamoto, T. Umeda, K. Watanabe, S. Onoda, M. Markham, D. Twitchen, B. Naydenov, L. McGuinness, T. Teraji, S. Koizumi, F. Dolde, H. Fedder, J. Honert, J. Wrachtrup, T. Ohshima, F. Jelezko, J. Isoya, Extending spin coherence times of diamond qubits by high-temperature annealing. *Phys. Rev. B* **88**, 075206 (2013).
25. E. Herbschleb, H. Kato, Y. Maruyama, T. Danjo, T. Makino, S. Yamasaki, I. Ohki, K. Hayashi, H. Morishita, M. Fujiwara, N. Mizuochi, Ultra-long coherence times amongst room-temperature solid-state spins. *Nat. Commun.* **10**, 3766 (2019).
26. X. Rong, J. Geng, F. Shi, Y. Liu, K. Xu, W. Ma, F. Kong, Z. Jiang, Y. Wu, J. Du, Experimental fault-tolerant universal quantum gates with solid-state spins under ambient conditions. *Nat. Commun.* **6**, 8748 (2015).
27. T. Xie, Z. Zhao, S. Xu, X. Kong, Z. Yang, M. Wang, Y. Wang, F. Shi, J. Du, 99.92%-fidelity cnot gates in solids by noise filtering. *Phys. Rev. Lett.* **130**, 030601 (2023).
28. V. M. Acosta, E. Bauch, M. P. Ledbetter, A. Waxman, L.-S. Bouchard, D. Budker, Temperature dependence of the nitrogen-vacancy magnetic resonance in diamond. *Phys. Rev. Lett.* **104**, 070801 (2010).
29. F. Dolde, H. Fedder, M. W. Doherty, T. Nöbauer, F. Rempp, G. Balasubramanian, T. Wolf, F. Reinhard, L. C. Hollenberg, F. Jelezko, J. Wrachtrup, Electric-field sensing using single diamond spins. *Nat. Phys.* **7**, 459–463 (2011).
30. M. Pompili, S. L. N. Hermans, S. Baier, H. K. C. Beukers, P. C. Humphreys, R. N. Schouten, R. F. L. Vermeulen, M. J. Tiggelman, L. dos Santos Martins, B. Dirkse, S. Wehner, R. Hanson, Realization of a multinode quantum network of remote solid-state qubits. *Science* **372**, 259–264 (2021).
31. N. Kalb, A. A. Reiserer, P. C. Humphreys, J. J. Bakermans, S. J. Kamerling, N. H. Nickerson, S. C. Benjamin, D. J. Twitchen, M. Markham, R. Hanson, Entanglement distillation between solid-state quantum network nodes. *Science* **356**, 928–932 (2017).
32. F. Shi, Q. Zhang, P. Wang, H. Sun, J. Wang, X. Rong, M. Chen, C. Ju, F. Reinhard, H. Chen, J. Wrachtrup, J. Wang, J. Du, Single-protein spin resonance spectroscopy under ambient conditions. *Science* **347**, 1135–1138 (2015).
33. I. Lovchinsky, A. Sushkov, E. Urbach, N. P. de Leon, S. Choi, K. De Greve, R. Evans, R. Gertner, E. Bersin, C. Müller, L. McGuinness, F. Jelezko, R. L. Walsworth, H. Park, M. D. Lukin, Nuclear magnetic resonance detection and spectroscopy of single proteins using quantum logic. *Science* **351**, 836–841 (2016).
34. I. Gross, W. Akhtar, V. Garcia, L. Martínez, S. Chouaieb, K. Garcia, C. Carrétéro, A. Barthélémy, P. Appel, P. Maletinsky, J.-V. Kim, J. Y. Chauleau, N. Jaouen, M. Viret, M. Bibes, S. Fusil, V. Jacques, Real-space imaging of non-collinear antiferromagnetic order with a single-spin magnetometer. *Nature* **549**, 252–256 (2017).
35. J.-P. Tetienne, T. Hingant, J.-V. Kim, L. H. Diez, J.-P. Adam, K. Garcia, J.-F. Roch, S. Rohart, A. Thiaville, D. Ravelosona, V. Jacques, Nanoscale imaging and control of domain-wall hopping with a nitrogen-vacancy center microscope. *Science* **344**, 1366–1369 (2014).
36. J. F. Barry, J. M. Schloss, E. Bauch, M. J. Turner, C. A. Hart, L. M. Pham, R. L. Walsworth, Sensitivity optimization for NV-diamond magnetometry. *Rev. Mod. Phys.* **92**, 015004 (2020).

37. W. Pfaff, B. J. Hensen, H. Bernien, S. B. van Dam, M. S. Blok, T. H. Taminiau, M. J. Tiggelman, R. N. Schouten, M. Markham, D. J. Twitchen, R. Hanson, Unconditional quantum teleportation between distant solid-state quantum bits. *Science* **345**, 532–535 (2014).
38. E. Neu, P. Appel, M. Ganzhorn, J. Miguel-Sánchez, M. Lesik, V. Mille, V. Jacques, A. Tallaire, J. Achard, P. Maletinsky, Photonic nano-structures on (111)-oriented diamond. *Appl. Phys. Lett.* **104**, 153108 (2014).
39. L. Jiang, J. S. Hodges, J. R. Maze, P. Maurer, J. M. Taylor, D. G. Cory, P. R. Hemmer, R. L. Walsworth, A. Yacoby, A. S. Zibrov, M. D. Lukin, Repetitive readout of a single electronic spin via quantum logic with nuclear spin ancillae. *Science* **326**, 267–272 (2009).
40. G. Waldherr, Y. Wang, S. Zaiser, M. Jamali, T. Schulte-Herbrüggen, H. Abe, T. Ohshima, J. Isoya, J. Du, P. Neumann, J. Wrachtrup, Quantum error correction in a solid-state hybrid spin register. *Nature* **506**, 204–207 (2014).
41. G. Waldherr, P. Neumann, S. F. Huelga, F. Jelezko, J. Wrachtrup, Violation of a temporal bell inequality for single spins in a diamond defect center. *Phys. Rev. Lett.* **107**, 090401 (2011).
42. B. J. Shields, Q. P. Unterreithmeier, N. P. de Leon, H. Park, M. D. Lukin, Efficient readout of a single spin state in diamond via spin-to-charge conversion. *Phys. Rev. Lett.* **114**, 136402 (2015).
43. J. M. Martinis, Qubit metrology for building a fault-tolerant quantum computer. *npj Quantum Inf.* **1**, 15005 (2015).
44. N. Aslam, G. Waldherr, P. Neumann, F. Jelezko, J. Wrachtrup, Photo-induced ionization dynamics of the nitrogen vacancy defect in diamond investigated by single-shot charge state detection. *New J. Phys.* **15**, 013064 (2013).
45. N. O. Antoniadis, M. R. Hogg, W. F. Stehl, A. Javadi, N. Tomm, R. Schott, S. R. Valentin, A. D. Wieck, A. Ludwig, R. J. Warburton, Cavity-enhanced single-shot readout of a quantum dot spin within 3 nanoseconds. *Nat. Commun.* **14**, 3977 (2023).
46. M. K. Bhaskar, R. Riedinger, B. Machielse, D. S. Levonian, C. T. Nguyen, E. N. Knall, H. Park, D. Englund, M. Lončar, D. D. Sukachev, M. D. Lukin, Experimental demonstration of memory-enhanced quantum communication. *Nature* **580**, 60–64 (2020).

Acknowledgments
Funding: This work was supported by the National Natural Science Foundation of China (grant nos. T2125011 and 12274396), the CAS (grant nos. GJJSTD20200001 and YSBR-068), the Innovation Program for Quantum Science and Technology (grants nos. 2021ZD0302200 and 2021ZD0303204), the Anhui Initiative in Quantum Information Technologies (grant no. AHY050000), the China Postdoctoral Science Foundation (grant nos. 2021M703110, 2022T150631, 2023M743399, and GZB20240718), and the Fundamental Research Funds for the Central Universities, New Cornerstone Science Foundation through the XPLORER PRIZE.
Author contributions: J.D., F.S., and T.X. supervised the project and proposed the idea. T.X., Z.Z., and F.S. designed the experiments. S.X., Z.Z., and Q.S. prepared the setup. M.W., P.Y., X.Y., Z.Y., and Y.W. prepared the diamond sample. Z.Z., T.X., and S.X. collected and analyzed the experiment data. T.X. and Z.Z. performed the derivation and simulation. Z.Z., T.X., and F.S. wrote the manuscript. All authors discussed the results and commented on the manuscript.
Competing interests: The authors declare that they have no competing interests. **Data and materials availability:** All data needed to evaluate the conclusions in the paper are present in the paper and/or the Supplementary Materials.

Submitted 18 April 2024
Accepted 1 November 2024
Published 6 December 2024
10.1126/sciadv.adp9228